

# Dynamic Reconstruction of Hand-Object Interaction with Distributed Force-aware Contact Representation

Zhenjun Yu<sup>\*</sup>, Wenqiang Xu<sup>\*</sup>, Pengfei Xie, Yutong Li, Cewu Lu<sup>§</sup>  
Shanghai Jiao Tong University

{jeffson-yu, vinjohn, pf.xie, davidliyutong, lucewu}@sjtu.edu.cn

## Abstract

We present *ViTaM-D*, a novel visual-tactile framework for dynamic hand-object interaction reconstruction, integrating distributed tactile sensing for more accurate contact modeling. While existing methods focus primarily on visual inputs, they struggle with capturing detailed contact interactions such as object deformation. Our approach leverages distributed tactile sensors to address this limitation by introducing *DF-Field*. This distributed force-aware contact representation models both kinetic and potential energy in hand-object interaction. *ViTaM-D* first reconstructs hand-object interactions using a visual-only network, *VDT-Net*, and then refines contact details through a force-aware optimization (*FO*) process, enhancing object deformation modeling. To benchmark our approach, we introduce the *HOT* dataset, which features 600 sequences of hand-object interactions, including deformable objects, built in a high-precision simulation environment. Extensive experiments on both the *DexYCB* and *HOT* datasets demonstrate significant improvements in accuracy over previous state-of-the-art methods such as *gSDF* and *HOTrack*. Our results highlight the superior performance of *ViTaM-D* in both rigid and deformable object reconstruction, as well as the effectiveness of *DF-Field* in refining hand poses. This work offers a comprehensive solution to dynamic hand-object interaction reconstruction by seamlessly integrating visual and tactile data. Codes, models, and datasets will be available.

## 1. Introduction

Human manipulates objects with tactile feedback. Reconstructing the manipulation process of hand-object interaction is an important task that can benefit many downstream tasks, such as VR/AR, robot imitation learning, and human behavior understanding. Previous works [4, 12, 27, 31, 34] on dynamic hand-object interaction reconstruction are pri-

marily visual-only. Visual-only methods can recover the global geometry and poses of hand and object, but they struggle with contact details such as object deformation due to a lack of information near contact areas.

Recently, visual-tactile methods [23, 28, 29] have increasingly drawn attention in hand-object reconstruction tasks, with the development of tactile sensing techniques [16, 21, 24, 37], which can supplement the perceptual ability near contact areas (Fig. 1.a). Among the fast-developing tactile sensors, distributed tactile sensors (Fig. 1.b) [16, 24, 36], which are wearable or attachable to a hand and allow collecting tactile information in a natural human-like hand-object interaction process, are more promising in human manipulation data collection than other types of tactile sensors [15, 21, 25, 37]. However, how to integrate such sensors with visual perception to reconstruct the states of hand-object interaction is seldom explored.

Due to the conformality between the distributed tactile sensor and the hand, the hand geometry will not be significantly influenced during manipulation. Therefore, we can use the same visual-only approach to reconstruct the hand-object state and integrate the tactile information to refine the result. Based on this observation, we propose a novel **Distributed Force-aware contact representation, DF-Field**, and a **Visual-Tactile Manipulation reconstruction framework with Distributed tactile sensing, ViTaM-D**. *DF-Field* models the contact by considering both kinetic and potential energy in hand-object interaction, which allows modeling object deformation. With this representation, *ViTaM-D* first reconstructs the hand-object interaction with visual-only observations by the proposed **Visual Dynamic Tracking network, VDT-Net**, and refines the contact details with *DF-Field* via a **Force-aware hand-pose Optimization process, FO**. Such design allows us to inherit the wisdom of fast-growing visual-only hand-object reconstruction methods [4, 12, 27, 34] and easily integrate the tactile information into an existing motion capture or estimation system.

To train the *VDT-Net*, we need large-scale hand-object interaction datasets since previous datasets [3, 9, 33] of hand-object interactions mostly cover rigid or articulated

<sup>\*</sup> indicates equal contributions.

<sup>§</sup> Cewu Lu is the corresponding author.

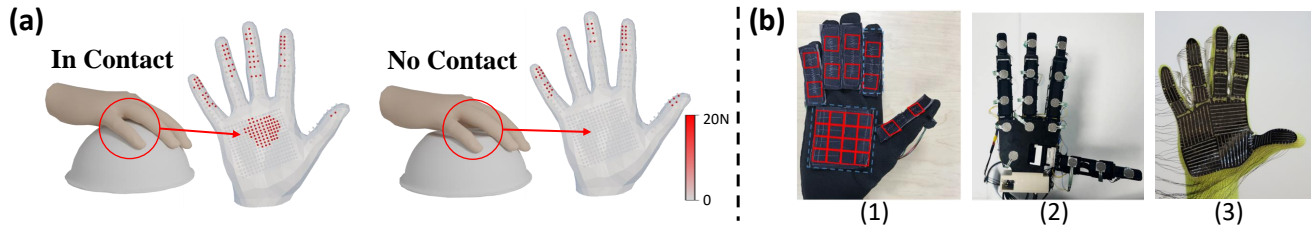


Figure 1. (a): The relationship between tactile information and contact geometry. Grasping different bowls with the same hand poses shows that the distributed tactile arrays can capture occlusion contacts and object states. (b): Different types of distributed tactile sensors proposed in previous works (1). [16], (2). [36], (3). [24].

object manipulation, failing to contain deformable objects. And they generally do not provide accurate tactile readings. Therefore, aside from the public dataset, DexYCB [3], which we adopt to benchmark on rigid objects with common baselines, we also create a new dataset, **HOT dataset**, to fully benchmark our method on deformable object reconstruction. The dataset is built with ZeMa [8], a high-precision physics-based simulation environment that supports penetration-free frictional contact modeling with finite element method (FEM) to model the object deformation. The HOT dataset contains 600 sequences of hand-object interaction, with 30 deformable objects from 5 different categories and 8 camera views for each sequence.

To evaluate the method, we compare our proposed ViTaM-D with previous state-of-the-art methods gSDF [6] and HOTrack [4] on DexYCB. Extensive experiments proved that our method realizes great improvements in the previous works both quantitatively and qualitatively. Besides, we also prove the great capability of our method in tracking deformable objects on the HOT Dataset and the effectiveness of the FO optimization in refining hand poses from penetrations and bad contact states.

Our contributions are summarized as follows:

(1) A visual-tactile learning framework, ViTaM-D. It contains a visual-only dynamic tracking network, VDT-Net, for reconstructing hand-object interactions and a force-aware optimization process, FO, to integrate the tactile information into reconstruction refinement based on a novel distributed force-aware contact representation, DF-Field.

(2) A new dataset, HOT. It contains 600 RGB-D manipulation sequences on 30 deformable objects from 5 categories with penetration-free hand-object poses and accurate tactile information.

## 2. Related Work

Hand-object reconstruction has been richly studied because it tries to recover the full details of hand-object interaction, showing potential applicability for downstream tasks.

Research in this direction starts with static reconstruction. Earlier works have predominantly relied on RGB in-

puts to estimate hand pose and object geometry. Hasson et al. [11] presented a method that learns hand-object interaction using synthetic RGB images with the grasp poses planned by GraspIt! [18]. Doosti et al. [7] proposed a graph-based network for hand-object pose estimation. Cao et al. [2] introduced a method that operates in-the-wild, estimating the hand pose first and optimizing the solution using a contact representation. The optimization involves push and pull terms to handle the contact, which is purely empirical. Similarly, CPF [31, 34] employs a contact representation using a spring-mass system, adopting an empirical approach to refine the hand-object interaction. ArtiBoost [32] further enhanced the performance of static hand-object reconstruction through data augmentation techniques. AlignSDF [5] leveraged RGB inputs to estimate hand pose and combined point cloud data for object geometry, using SDF-based decoders for both hand and object reconstruction.

Later, hand-object reconstruction in the dynamic setting draws increasing attention since manipulation is naturally dynamic. Approaches have advanced by incorporating temporal information and using more complex representations. Tekin et al. [26] adopted RNN for temporal feature fusion, utilizing egocentric RGB video to capture dynamic hand-object interaction and pose estimation. Hasson et al. [13] improved dynamic reconstruction by enforcing photometric consistency constraints. Ye et al. [35] introduced a diffusion model that guides dynamic hand-object reconstruction via score distillation sampling and differentiable rendering techniques. Recent advances by Fan et al. [10] focused on refining pose estimation using SDF-based representations and volumetric rendering, improving the overall dynamic reconstruction accuracy. Furthermore, gSDF [6] employed transformer architectures and SDF representations to model complex hand-object interactions dynamically.

These works focus more on visual-only inputs. However, due to occlusion between the hand and object during the interaction, visual perception usually lacks information near the contact areas, and such information cannot necessarily be mitigated by cross-frame feature fusion. Therefore, tactile perception comes to supplement the near-contact in-

formation. Zhang et al. [38] utilized a tactile glove [24] to track object movements. However, it focuses more on the dynamic object trajectory rather than contact geometry. Works such as [23, 28] employed optical tactile sensors, trained the model by synthetic data, and applied to rigid object geometry reconstruction. Later, VTacO [29] extended this line of research by using optical tactile sensors to capture object geometry, including deformation, providing a more comprehensive representation of hand-object interactions. Unlike these works, the proposed ViTaM-D inherits the merits from both worlds; it leverages the advanced techniques of visual-only reconstruction and incorporates the distributed tactile readings to enhance the local contact details.

### 3. Force-aware Contact Representation

During manipulation, forces from the hand change both hand and object states. To fully capture dynamic contact behaviors, the representation must encode both contact locations and forces. We introduce a distributed force-aware contact representation, **DF-Field** (Sec. 3.1), and apply it using distributed tactile sensors (Sec. 3.2).

#### 3.1. DF-Field Representation

Without loss of generality, we take the object-centric perspective to describe a hand-object interaction process, where the object is assumed to be fixed in the origin point, and the hand moves around the object. In this way, by ignoring the gravitational potential energy, the contact dynamics in a manipulation process are driven by the **Relative Potential Energy**, which is the resulting energy of the kinetic energy and deformation potential energy of the hand and object. Besides, we assume a virtual **Barrier Energy** lies between the hand and object contact surface to prevent penetration. With an established point pair  $i, j$  of object vertex  $\mathcal{V}_i^o$  and hand vertex  $\mathcal{V}_j^h$ , and the Euclidean distance of the point pair  $l_{ij} = \|\mathcal{V}_i^o - \mathcal{V}_j^h\|_2$ , we define the two energy terms as follows.

**Relative Potential Energy.** A relative potential energy that describes both the object deformation and the hand movements:

$$E_{ij} = \kappa l_{ij}^2, \quad (1)$$

where  $\kappa$  is a parameter representing the hand interacting with the object vertices. If  $\kappa > 0$ , the hand and object are in contact. Thus, the distance  $l_{ij}$  and the relative energy will be close to 0, indicating that the contact’s relative potential energy is satisfied.

**Barrier Energy.** Given a certain threshold distance  $\hat{l}$ , the barrier energy is:

$$B_{ij} = \begin{cases} -e^{-\kappa(l_{ij} - \hat{l})^2} \log\left(\frac{l_{ij}}{\hat{l}}\right), & 0 < l_{ij} < \hat{l} \\ 0 & l_{ij} \geq \hat{l} \end{cases} \quad (2)$$

This barrier energy aims to push away the point pair when  $\kappa$  is low, thus avoiding penetration issues between the hand and object. The function is defined in this way not only to ensure repulsion becomes smaller when the distance is larger but also to remain smooth for optimization.

**Overall Energy.** A proper contact is met when both energy terms approach 0:

$$E = \sum_i \sum_j (E_{ij} + B_{ij}). \quad (3)$$

To note, though  $\kappa$  is strongly correlated to the tactile readings, DF-Field can also be tactile-independent, as long as we empirically set the exerted force instead of physics-based. In this way, DF-Field can work with visual-only methods. Different setups of force are discussed in Sec. 6.5.

#### 3.2. DF-Field with Distributed Tactile Sensors

As aforementioned, the distributed tactile sensors generally conform to the hand, and different tactile sensors may have different layout configurations. Thus, to adapt to different tactile sensors, we take the hand-centric perspective by first dividing the hand into 22 regions (as shown in the left of Fig. 3.a, 2 areas for the thumb, 3 for other fingers, and 8 for the palm), and assign the tactile sensors to the corresponding region. In each region, we define the center as the hand keypoint, resulting in  $\mathcal{K}^h \in \mathbb{R}^{22 \times 3}$ .

For optimization, we connect only the hand keypoints to object vertices, reducing computational load while enhancing regional interaction information. The force in each region is calculated by averaging the tactile readings  $\mathcal{M}^j$ , and by the definition of the energy, we can obtain that  $\kappa$  is the difference of the exerted force over the distance  $l_{ij}$ . In practice, we approximate it by dividing the force by the distance:

$$\kappa_{ij} \sim \frac{\overline{\mathcal{M}^j}}{l_{ij}}. \quad (4)$$

We will discuss the difference between choosing keypoints or all-hand vertices for optimization in Sec. Appendix B.2.

## 4. ViTaM-D Method

### 4.1. Overview

We address the problem of 4D tracking and dynamic reconstruction of hand-object interactions from a visual-tactile perspective and propose a novel method named **ViTaM-D**. We assume that the visual input consists of a live stream of 3D point clouds, denoted as  $\{\mathcal{P}_t \in \mathbb{R}^{N \times 3}\}_{t=1}^n$ , representing hand-object interactions derived from single-view depth images, where  $N$  is the number of input point. The tactile input  $\{\mathcal{M}_t\}_{t=1}^n$  contains distributed tactile sensor readings for each frame.

**ViTaM-D** tracks hand-object states in two stages: Visual Dynamic Tracking (**VDT-Net**) and Force-aware Optimization (**FO**). **VDT-Net** uses visual-only inputs to establish flow features and dynamically reconstruct the hand and object, capturing global hand-object geometry but struggling with sparse contact region details. To address this, the second stage, **FO**, incorporates tactile information to improve contact accuracy and reduce penetration issues. The overall pipeline is given in Fig. 2.

## 4.2. Visual Dynamic Tracking of hand and object, VDT-Net

In the first stage, the VDT-Net first predicts the flow from the last to the current frame with a flow prediction module and extracts a fused visual feature from the current frame’s flow and point cloud. This feature will then be forwarded into **Object Decoder** and **Hand Decoder** to reconstruct the object and hand geometry, respectively. We use the Signed Distance Field (SDF) to model the objects and the MANO model [22] for the hand.

**Flow Prediction Module.** At frame  $t$ , we first extract the per-point features  $F_t, F_{t-1} \in \mathbb{R}^{N \times d}$  from  $\mathcal{P}_t$  and  $\mathcal{P}_{t-1}$  using a backbone network  $I(\cdot)$ . In practice, we adopt a simple PointNet++ [20] for feature extraction, with 3 layers of set abstraction and 3 layers of feature propagation. Then, we design a flow prediction network  $\mathcal{F}_f(\cdot)$  to predict the point cloud flow  $f_{t-1 \rightarrow t} \in \mathbb{R}^{N \times 3}$  from frame  $t-1$  to  $t$ , which contains the correspondence information between the two frames and represents the hand movement and object deformation:

$$f_{t-1 \rightarrow t} = \mathcal{F}_f(F_t, F_{t-1}, \mathcal{P}_t, \mathcal{P}_{t-1}). \quad (5)$$

In  $\mathcal{F}_f$ , we first perform a Cartesian product of the two extracted features, yielding a tensor of size  $N \times N \times 2d$ . This tensor is fed into a 3-layer MLP to obtain  $\mathcal{C}_v$ , which is then used in two ways. First, it passes through a 2D convolutional layer for downsampling to obtain  $p_c \in \mathbb{R}^{N \times N}$ , representing the matching probability of each point between two frames. Second,  $\mathcal{C}_v$  is sent through a softmax function and a one-layer MLP to downsample, resulting in  $\mathcal{C}_c \in \mathbb{R}^N$ , indicating whether the points in the first frame are matched in the second frame. Thus, the final matching probability matrix  $p_m \in \mathbb{R}^{N \times N}$ , which describes the correspondence likelihood between the two point sets, can be computed as:

$$p_m = p_c \times \mathcal{C}_c \quad (6)$$

After estimating the matching probability, we compute the disparity of two point cloud sets  $\mathcal{D} \in \mathbb{R}^{N \times N \times 3}$ , with  $D_{ij} = \mathcal{P}_t^i - \mathcal{P}_{t-1}^j$ , and concatenate the disparity with  $p_m$ . The concatenated tensor is then fed into four 2D convolutional layers with batch normalization and a softmax function to obtain the disparity feature  $F_d \in \mathbb{R}^{N \times d'}$ . Finally, we

use PointNet++ [20] to regress the flow  $f_{t-1 \rightarrow t} \in \mathbb{R}^{N \times 3}$ . The flow prediction results will be discussed in Appendix B.1.

Additionally, we use another PointNet++  $I'(\cdot)$  to extract the visual correspondence feature  $F_t^f$  from  $\mathcal{P}_{t-1}$  with  $f_{t-1 \rightarrow t}$  added.  $F_t^f$  and  $F_t$  are then forwarded to a transformer fusion module to obtain the final visual feature  $F_v$ , corresponding to the current frame’s point cloud  $\mathcal{P}_t$ . Specifically, the transformer fusion module first uses a self-attention module to encode the point cloud features from both frames. After applying positional embedding between the feature and its point cloud, a cross-attention module fuses the two features and outputs the final visual feature. This fusion strategy considers both the 3D static information of the current frame and the corresponding feature extracted from the flow.

**Object Decoder.** Based on the final visual feature  $F_v$ , the **Object Decoder** follows two steps: **Feature Scattering & Sampling**, and **SDF Decoding**, to obtain the SDF predictions and the object mesh using Marching Cubes algorithm [17]. We follow the design in ConvOccNet [19], which scatters the feature into volume with the resolution  $D$ , feeds it into a 3D-UNet, and finally uses a 5-layer MLP to predict the signed distance for every point.

**Hand Decoder.** For hand tracking and reconstruction, we adopt the parametric MANO hand model [22], which uses  $\beta \in \mathbb{R}^{10}$  for hand shape, and  $\theta \in \mathbb{R}^{51}$  for hand poses.

Based on the extracted final visual feature  $F_v$ , and the point cloud  $\mathcal{P}_{t-1}$  of the last frame as input, we inherit a voting mechanism in PVN3D [14] to predict the hand joint positions  $\mathcal{J}_h \in \mathbb{R}^{21 \times 3}$  of the current frame. Besides predicting the translation offset  $\mathcal{O}_t \in \mathbb{R}^{21 \times 3}$ , we also predict the initial position of the keypoint by estimating a probability matrix  $T_{t-1} \in \mathbb{R}^{N \times 21}$  and multiply it with the former frame point cloud  $\mathcal{P}_{t-1}$ . The final prediction of the hand joint locations  $\mathcal{J}_h$  is:

$$\mathcal{J}_h = \mathcal{O}_t + \mathcal{P}_{t-1} \times T_{t-1} \quad (7)$$

After obtaining hand joint locations  $\mathcal{J}_h$ , we use the inverse kinematics method [39] to find the joint poses  $\theta$  with a template hand shape  $\beta$ , and we can easily reconstruct the hand mesh through a differentiable MANO layer.

**Loss Function.** We train the network in an end-to-end way, and optimize the framework parameters with three loss terms:

$$\mathcal{L} = \lambda_f \mathcal{L}_{flow} + \lambda_s \mathcal{L}_{SDF} + \lambda_H \mathcal{L}_{Hand}, \quad (8)$$

where flow loss is defined by two Chamfer distance terms  $\mathcal{L}_{flow} = CD(\mathcal{P}'_{t-1}, \mathcal{P}_t) + CD(\mathcal{P}''_t, \mathcal{P}_{t-1})$ ,  $\mathcal{P}'_{t-1} = \mathcal{P}_{t-1} + f_{t-1 \rightarrow t}$  is the forward-shifted point cloud and  $\mathcal{P}''_t = \mathcal{P}_t + f_{t \rightarrow t-1}$  is the backward-shifted point cloud. SDF loss is  $\mathcal{L}_{SDF} = |s - s^*|$ , where  $s^*$  represents the ground truth of

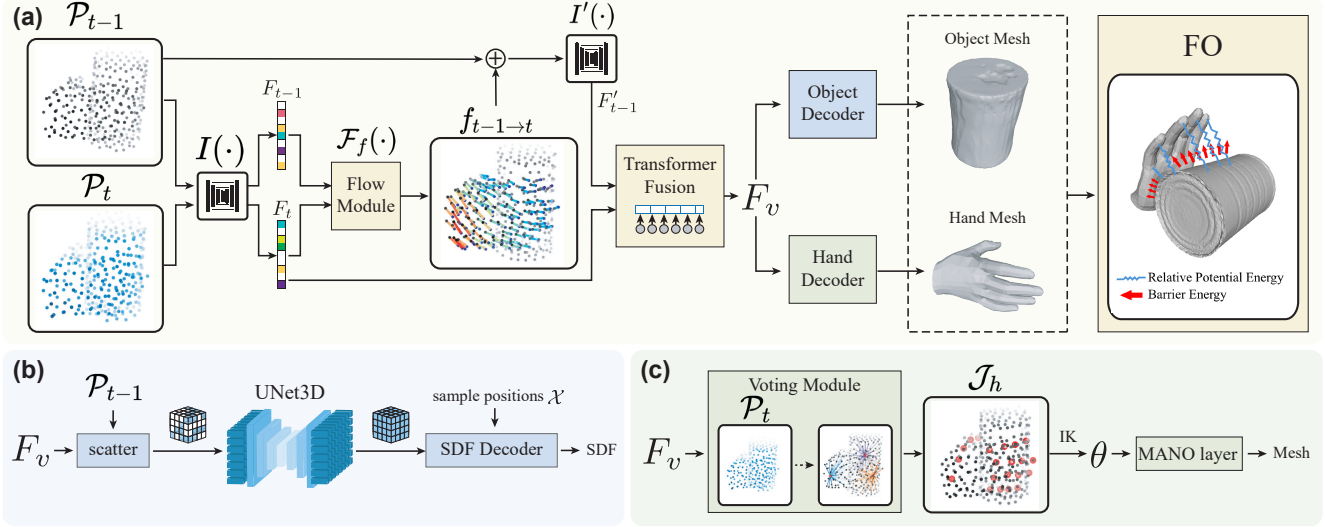


Figure 2. **ViTaM-D** pipeline. (a): The overview of our pipeline, including the flow prediction module for visual feature extraction and flow estimation, the Hand and Object Decoders, and Force-aware hand-pose Optimization, FO. (b): The Object Decoder to reconstruct the object mesh. (c): The Hand Decoder for estimating hand parameters and reconstructing based on the MANO model.

SDF. Hand joint loss is  $\mathcal{L}_{Hand} = \|\mathcal{J}_h - \mathcal{J}_h^*\|_2^2$ , with  $\mathcal{J}_h^*$  the ground truth of hand keypoints.

### 4.3. Force-aware Hand-pose Optimization, FO

After proper training, the VDT-Net, as well as other visual-only approaches, can give decent outputs of hand-object reconstruction. However, information near the contact areas is lacking due to self-occlusion, and the contact details should be further improved. Here, we describe an optimization method with force readings.

Given the contact energy defined in Sec. 3, we optimize the predicted pose  $\theta$  from the hand decoder, with respect to the reconstructed object mesh, to obtain a better hand mesh and contact state. Based on Equ. 3, we use the ball-query method to find the corresponding object vertices for each hand region with a radius  $R$ , and the point pair will be set up between them and the hand keypoints  $\mathcal{J}_h$ .

Besides, For a given joint  $j$ , we ensure it remains in reasonable poses by penalizing rotations  $\mathcal{R}_j$  that are near twisted directions  $\mathcal{R}_t$  or if any angle exceeds  $\pi/2$ , using the  $L_2$  loss. Additionally, we constrain the optimized hand pose  $^*\theta$  to stay close to the original prediction:

$$\mathcal{L}_r = \|\mathcal{R}_j \cdot \mathcal{R}_t\|_2^2 + \left\| \max(|\mathcal{R}_j| - \frac{\pi}{2}, 0) \right\|_2^2, \quad (9)$$

$$\mathcal{L}_o = \|^*\theta - \theta\|_2^2.$$

Finally, the optimization target can be demonstrated as:

$$^*\theta = \arg \min_{\theta} (E + \mathcal{L}_r + \mathcal{L}_o) \quad (10)$$

We use the gradient descent method and the Adam solver for optimization. By minimizing energy and loss, we can

obtain a better interaction state between the hand and object, avoid severe penetration problems, and forbid the hand from abnormal poses.

## 5. Hand-Object Tactile Dataset, HOT Dataset

Since obtaining the ground truth in the real world, such as object deformation, is relatively hard, previous works [3, 33] on hand-object interaction recording mainly focus on rigid or articulated objects. To fully benchmark our method’s ability on deformable objects, we also create **Hand-Object-Tactile dataset, HOT dataset**, which contains depth images, force sensor readings, and SDF ground truths generated by the simulation environment **ZeMa** [8] which realizes intersection-free and high accuracy of contact modeling and deformation based on FEM.

### 5.1. Data Acquisition

An example of collecting a training data sequence in the simulation environment is shown in Fig. 3.b. To ensure valid data points and stable grasps with multiple contacts between the objects and various regions of the hand, we use DiPGrasp [30], a fast and effective grasp planner. After obtaining a feasible grasp pose, we fix the selected object model, position the hand a certain distance from the final grasp translation, and add a slight perturbation to the final rotation. The hand is set fully open with joint states their lower limits. In the first stage, the hand moves slowly towards the final grasp transformation target. Next, we perform the grasp by gradually increasing the joint state values until they reach the grasp joint target. This process yields a complete training data sequence, including depth

images, point clouds, and tactile arrays  $\{\mathcal{P}_t, \mathcal{M}_t\}_{t=1}^n$  for each frame.

## 5.2. Dataset Statistics

In the **HOT** Dataset, we adopt objects from **YCB** [1] model repositories, which contain various object categories. We selected 5 to 10 different objects in the category **Bottle** and **Box** from the YCB dataset, and we manually added 5 **Sponges**, 5 **Plasticines**, and 5 **Stuffed Animals** to demonstrate the ability of our model to track objects with large deformations.

The simulator ZeMa mainly uses density  $\rho$ , Young’s modulus  $E$ , and Poisson’s ratio  $\nu$  to describe the properties of different deformable objects. We will therefore use the parameters of objects that correspond to reality. For the object in category **Bottle** and **Box**, we set  $\rho = 10^3 \text{kg/m}^3$ ,  $E = 1.271 \text{GPa}$ ,  $\nu = 0.28$ , and for the **Sponges**, **Plasticines** and **Stuffed Animals**,  $\rho = 30 \text{kg/m}^3$ ,  $E = 0.1 \text{MPa}$ ,  $\nu = 0.38$ . And as we consider **Plasticine** as plastic objects, we set its yield stress  $s_y = 200 \text{pa}$ .

For each object, we randomly generate 20 different trajectories, with 15 for training, 2 for testing, and 3 for validation and visualization. The whole dataset consists of 600 sequences which contains 50-100 frames, and each sequence involves 8 different views of camera for capturing point clouds.

## 6. Experiments

### 6.1. Implementation Details

We set the input point cloud size to  $N = 1024$ . We randomly sample  $1 \times 10^6$  positions in the space, including  $2 \times 10^5$  points on the object surface. By subsampling to  $M = 2048$ , we obtain the sample positions for SDF prediction during training. The point cloud feature size is set to  $d = 128$ , the disparity feature size to  $d' = 64$ , and the resolution of the volume feature for SDF decoding to  $D = 64$ . We empirically set the loss weights to  $\lambda_f = 0.01$ ,  $\lambda_S = 0.5$ , and  $\lambda_H = 1$ .

We first train our VDT-Net on the entire dataset with a batch size of 6 and a learning rate of  $1e-4$  using the Adam optimizer for 100 epochs. We then fine-tune each object category with a batch size of 4 and a learning rate of  $5e-5$  for 50-100 epochs, depending on the number of objects. The training process takes 15 hours on an Nvidia A40 GPU.

For the FO process, we set the threshold distance in the barrier function to  $\hat{l} = 2 \text{mm}$  and the ball-query radius for finding object vertices to  $R = 5 \text{mm}$ . We minimize the energy function for 100 iterations per frame with a learning rate of  $2e-3$  using the Adam solver. It takes approximately  $3.5 \pm 0.5$  seconds per frame to complete refinement.

### 6.2. Datasets

To train and evaluate our method, we first use the dataset **DexYCB**, which captures hand grasping of rigid objects, with RGB-D cameras recorded. It can directly validate our method’s capability against the baselines. In addition, we use the **HOT** dataset, which contains interactions of hand and deformable objects with rich and accurate tactile information. It can evaluate the ability of our method to track object deformation and the effectiveness of our designed force-aware contact representation.

### 6.3. Metrics

**Intersection over Union (IoU)** evaluates the intersection percentage between the predicted object mesh and the ground truth.

**Chamfer Distance (CD)** assesses the reconstruction accuracy of object vertices.

**Mean Per Joint Position Error (MPJPE)** evaluates the accuracy of hand joint location tracking.

**Penetration Depth (PD)** measures the physical plausibility of hand-object interaction by reporting the maximum distance of hand penetration into the object.

**Hand-Object Contact Mask IoU (CIoU)** validates the contact recovery of hand-pose optimization by measuring the IoU of the contact mask between the optimized hand-object state and the ground truth. Contacts are defined as distances less than 3mm between hand and object vertices.

### 6.4. Results

For hand-object tracking evaluation, we compare our results with the state-of-the-art methods gSDF [6] and HO-Track [4]. gSDF uses RGB images to reconstruct objects with SDF representation, while HOTrack uses segmented point clouds to predict object poses. Our method uses unsegmented point clouds as input and output object meshes, making it more challenging to achieve better results. Additionally, since these baselines only work with rigid objects, we compare them only with the DexYCB object categories. DexYCB does not provide tactile information, so we only use VDT-Net to compare with the baseline methods here. Later, we provide an empirical way to use FO with a fixed force setting, which will be discussed in Sec. 6.5.

The quantitative results are shown in Tab. 1. In the DexYCB dataset, our leading scores in IoU and Chamfer distance demonstrate superior object tracking and reconstruction capabilities. Additionally, our higher MPJPE score indicates better hand-tracking performance. gSDF’s better performance on penetration depth is due to occasional incomplete object reconstruction, as illustrated in Fig. 4, where the pitcher is missing its handle. For the HOT dataset, VDT-Net achieves excellent scores. Significant improvements in MPJPE, PD, and CIoU after applying



Metrics	IoU(%) $\uparrow$	CD(mm) $\downarrow$	MPJPE(mm) $\downarrow$	PD(mm) $\downarrow$	CIoU(%) $\uparrow$
DexYCB					
gSDF	86.8	13.4	14.4	<b>8.9</b>	31.3
HOTTrack	88.2	10.2	25.7	12.3	28.5
Ours (VDT)	<b>90.1</b>	<b>9.6</b>	<b>13.2</b>	9.9	<b>35.4</b>
HOT					
Ours (VDT)	80.5	10.9	13.6	10.7	29.8
Ours (VDT + FO)	*	*	<b>11.3</b>	<b>7.3</b>	<b>40.3</b>

Table 1. Quantitative results on DexYCB and HOT datasets for previous SOTA and our method. We only compare our results on rigid objects with the baselines. \* indicates that adding FO doesn't impact the metrics on reconstructed objects.  $\uparrow$  /  $\downarrow$  indicates higher scores/lower scores are better.

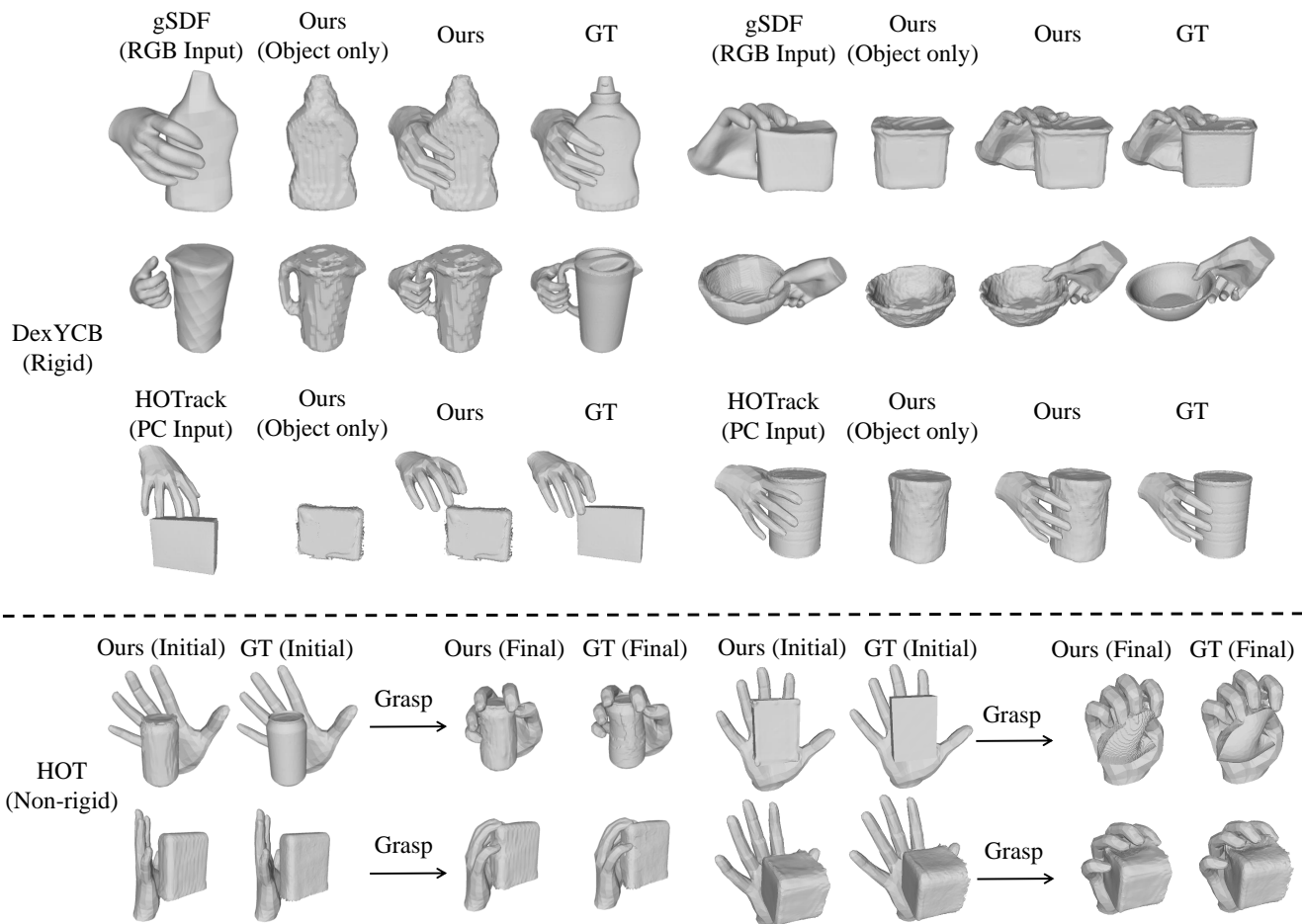


Figure 4. Qualitative results on both DexYCB and HOT datasets. The upper shows our better performances on rigid objects compared to the baselines, and the lower demonstrates the effectiveness of VDT-Net in dynamic reconstruction for deformable objects and hands.

human-robot collaboration.

## References

- [1] Berk Calli, Arjun Singh, Aaron Walsman, Siddhartha Srinivasa, Pieter Abbeel, and Aaron M Dollar. The ycb object and model set: Towards common benchmarks for manipula-

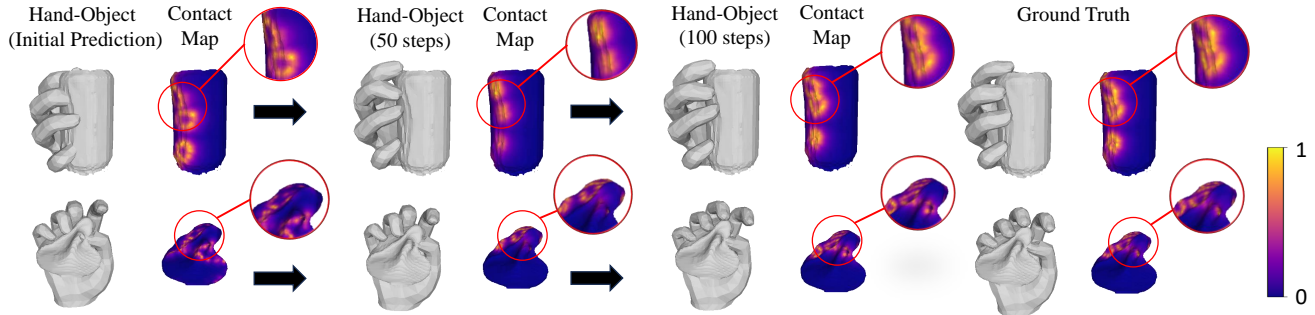


Figure 5. Qualitative results with FO. As iteration steps rise, the penetration problem decreases, and the contact map is closer to the ground truth, making the contact more reasonable.

Metrics	IoU(%) $\uparrow$	CD(mm) $\downarrow$
VDT	80.5	<b>10.9</b>
VDT with Tactile	<b>81.2</b>	11.5

Table 2. Quantitative results for whether or not fusing tactile information in VDT-Net.

Metrics	MPJPE	PD	CIoU
DexYCB			
VDT	13.2	9.9	35.4
VDT+FO( $\mathcal{M}$ fix)	<b>12.3</b>	<b>8.5</b>	<b>39.7</b>
HOT			
VDT+FO( $\mathcal{M}$ fix)	12.9	8.5	36.8
VDT+FO	<b>11.3</b>	<b>7.3</b>	<b>40.3</b>

Table 3. Quantitative results for different force representations.

- tion research. In *2015 international conference on advanced robotics (ICAR)*, pages 510–517. IEEE, 2015. **6**
- [2] Zhe Cao, Ilija Radosavovic, Angjoo Kanazawa, and Jitendra Malik. Reconstructing hand-object interactions in the wild. In *Proceedings of the IEEE/CVF International Conference on Computer Vision*, pages 12417–12426, 2021. **2**
- [3] Yu-Wei Chao, Wei Yang, Yu Xiang, Pavlo Molchanov, Ankur Handa, Jonathan Tremblay, Yashraj S Narang, Karl Van Wyk, Umar Iqbal, Stan Birchfield, et al. Dexycb: A benchmark for capturing hand grasping of objects. In *Proceedings of the IEEE/CVF Conference on Computer Vision and Pattern Recognition*, pages 9044–9053, 2021. **1, 2, 5**
- [4] Jiayi Chen, Mi Yan, Jiazhao Zhang, Yinzhen Xu, Xiaolong Li, Yijia Weng, Li Yi, Shuran Song, and He Wang. Tracking and reconstructing hand object interactions from point cloud sequences in the wild. In *Proceedings of the AAAI Conference on Artificial Intelligence*, pages 304–312, 2023. **1, 2, 6**
- [5] Zerui Chen, Yana Hasson, Cordelia Schmid, and Ivan Laptev. Alignsdf: Pose-aligned signed distance fields for hand-object reconstruction. In *European Conference on Computer Vision*, pages 231–248. Springer, 2022. **2**
- [6] Zerui Chen, Shizhe Chen, Cordelia Schmid, and Ivan Laptev. gsdf: Geometry-driven signed distance functions for 3d hand-object reconstruction. In *Proceedings of the IEEE/CVF Conference on Computer Vision and Pattern Recognition*, pages 12890–12900, 2023. **2, 6**
- [7] Bardia Doosti, Shujon Naha, Majid Mirbagheri, and David J Crandall. Hope-net: A graph-based model for hand-object pose estimation. In *Proceedings of the IEEE/CVF conference on computer vision and pattern recognition*, pages 6608–6617, 2020. **2**
- [8] Wenxin Du, Siqiong Yao, Xinlei Wang, Yuhang Xu, Wenqiang Xu, and Cewu Lu. Intersection-free robot manipulation with soft-rigid coupled incremental potential contact. *IEEE Robotics and Automation Letters*, 2024. **2, 5**
- [9] Zicong Fan, Omid Taheri, Dimitrios Tzionas, Muhammed Kocabas, Manuel Kaufmann, Michael J Black, and Otmar Hilliges. Arctic: A dataset for dexterous bimanual hand-object manipulation. In *Proceedings of the IEEE/CVF Conference on Computer Vision and Pattern Recognition*, pages 12943–12954, 2023. **1**
- [10] Zicong Fan, Maria Pirelli, Maria Eleni Kadoglou, Xu Chen, Muhammed Kocabas, Michael J Black, and Otmar Hilliges. Hold: Category-agnostic 3d reconstruction of interacting hands and objects from video. In *Proceedings of the IEEE/CVF Conference on Computer Vision and Pattern Recognition*, pages 494–504, 2024. **2**
- [11] Yana Hasson, Gul Varol, Dimitrios Tzionas, Igor Kalevatykh, Michael J Black, Ivan Laptev, and Cordelia Schmid. Learning joint reconstruction of hands and manipulated objects. In *Proceedings of the IEEE/CVF conference on computer vision and pattern recognition*, pages 11807–11816, 2019. **2**
- [12] Yana Hasson, Gul Varol, Dimitrios Tzionas, Igor Kalevatykh, Michael J Black, Ivan Laptev, and Cordelia Schmid. Learning joint reconstruction of hands and manipulated objects. In *Proceedings of the IEEE/CVF conference on com-*

- puter vision and pattern recognition, pages 11807–11816, 2019. 1
- [13] Yana Hasson, Bugra Tekin, Federica Bogo, Ivan Laptev, Marc Pollefeys, and Cordelia Schmid. Leveraging photometric consistency over time for sparsely supervised hand-object reconstruction. In *Proceedings of the IEEE/CVF conference on computer vision and pattern recognition*, pages 571–580, 2020. 2
- [14] Yisheng He, Wei Sun, Haibin Huang, Jianran Liu, Haoqiang Fan, and Jian Sun. Pvn3d: A deep point-wise 3d keypoints voting network for 6dof pose estimation. In *Proceedings of the IEEE/CVF conference on computer vision and pattern recognition*, pages 11632–11641, 2020. 4
- [15] Mike Lambeta, Po-Wei Chou, Stephen Tian, Brian Yang, Benjamin Maloon, Victoria Rose Most, Dave Stroud, Raymond Santos, Ahmad Byagowi, Gregg Kammerer, et al. Digit: A novel design for a low-cost compact high-resolution tactile sensor with application to in-hand manipulation. *IEEE Robotics and Automation Letters*, 5(3):3838–3845, 2020. 1
- [16] Hangxin Liu, Xu Xie, Matt Millar, Mark Edmonds, Feng Gao, Yixin Zhu, Veronica J Santos, Brandon Rothrock, and Song-Chun Zhu. A glove-based system for studying hand-object manipulation via joint pose and force sensing. In *2017 IEEE/RSJ International Conference on Intelligent Robots and Systems (IROS)*, pages 6617–6624. IEEE, 2017. 1, 2
- [17] William E Lorensen and Harvey E Cline. Marching cubes: A high resolution 3d surface construction algorithm. *ACM TOG*, 21(4):163–169, 1987. 4
- [18] Andrew T Miller and Peter K Allen. Graspit! a versatile simulator for robotic grasping. *IEEE Robotics & Automation Magazine*, 11(4):110–122, 2004. 2
- [19] Songyou Peng, Michael Niemeyer, Lars Mescheder, Marc Pollefeys, and Andreas Geiger. Convolutional occupancy networks. In *Computer Vision—ECCV 2020: 16th European Conference, Glasgow, UK, August 23–28, 2020, Proceedings, Part III 16*, pages 523–540. Springer, 2020. 4
- [20] Charles Ruizhongtai Qi, Li Yi, Hao Su, and Leonidas J Guibas. Pointnet++: Deep hierarchical feature learning on point sets in a metric space. *Advances in neural information processing systems*, 30, 2017. 4
- [21] Jieji Ren, Jiang Zou, and Guoying Gu. Mc-Tac: Modular camera-based tactile sensor for robot gripper. In *The 16th International Conference on Intelligent Robotics and Applications (ICIRA)*, 2023. 1
- [22] Javier Romero, Dimitrios Tzionas, and Michael J. Black. Embodied hands: Modeling and capturing hands and bodies together. *ACM Transactions on Graphics, (Proc. SIGGRAPH Asia)*, 2017. 4
- [23] Edward Smith, Roberto Calandra, Adriana Romero, Georgia Gkioxari, David Meger, Jitendra Malik, and Michal Drozdal. 3d shape reconstruction from vision and touch. *Advances in Neural Information Processing Systems*, 33: 14193–14206, 2020. 1, 3
- [24] Subramanian Sundaram, Petr Kellnhofer, Yunzhu Li, Jun-Yan Zhu, Antonio Torralba, and Wojciech Matusik. Learning the signatures of the human grasp using a scalable tactile glove. *Nature*, 569(7758):698–702, 2019. 1, 2, 3, 7
- [25] Ian H Taylor, Siyuan Dong, and Alberto Rodriguez. Gelslim 3.0: High-resolution measurement of shape, force and slip in a compact tactile-sensing finger. In *2022 International Conference on Robotics and Automation (ICRA)*, pages 10781–10787. IEEE, 2022. 1
- [26] Bugra Tekin, Federica Bogo, and Marc Pollefeys. H+ o: Unified egocentric recognition of 3d hand-object poses and interactions. In *Proceedings of the IEEE/CVF conference on computer vision and pattern recognition*, pages 4511–4520, 2019. 2
- [27] Aggeliki Tsoli and Antonis A Argyros. Joint 3d tracking of a deformable object in interaction with a hand. In *Proceedings of the European Conference on Computer Vision (ECCV)*, pages 484–500, 2018. 1
- [28] Shaoxiong Wang, Jiajun Wu, Xingyuan Sun, Wenzhen Yuan, William T Freeman, Joshua B Tenenbaum, and Edward H Adelson. 3d shape perception from monocular vision, touch, and shape priors. In *2018 IEEE/RSJ International Conference on Intelligent Robots and Systems (IROS)*, pages 1606–1613. IEEE, 2018. 1, 3
- [29] Wenqiang Xu, Zhenjun Yu, Han Xue, Ruolin Ye, Siqiong Yao, and Cewu Lu. Visual-tactile sensing for in-hand object reconstruction. In *CVPR IEEE Conference on Computer Vision and Pattern Recognition*, pages 8803–8812, 2023. 1, 3
- [30] Wenqiang Xu, Jieyi Zhang, Tutian Tang, Zhenjun Yu, Yutong Li, and Cewu Lu. Dipgrasp: Parallel local searching for efficient differentiable grasp planning. *IEEE Robotics and Automation Letters*, 2024. 5
- [31] Lixin Yang, Xinyu Zhan, Kailin Li, Wenqiang Xu, Jiefeng Li, and Cewu Lu. Cpf: Learning a contact potential field to model the hand-object interaction. In *ICCV IEEE/CVF International Conference on Computer Vision*, pages 11097–11106, 2021. 1, 2
- [32] Lixin Yang, Kailin Li, Xinyu Zhan, Jun Lv, Wenqiang Xu, Jiefeng Li, and Cewu Lu. Artiboost: Boosting articulated 3d hand-object pose estimation via online exploration and synthesis. In *Proceedings of the IEEE/CVF conference on computer vision and pattern recognition*, pages 2750–2760, 2022. 2
- [33] Lixin Yang, Kailin Li, Xinyu Zhan, Fei Wu, Anran Xu, Liu Liu, and Cewu Lu. Oakink: A large-scale knowledge repository for understanding hand-object interaction. In *Proceedings of the IEEE/CVF Conference on Computer Vision and Pattern Recognition*, pages 20953–20962, 2022. 1, 5
- [34] Lixin Yang, Xinyu Zhan, Kailin Li, Wenqiang Xu, Jiefeng Li, and Cewu Lu. Learning a contact potential field for modeling the hand-object interaction. *IEEE Transactions on Pattern Analysis and Machine Intelligence*, 2024. 1, 2
- [35] Yufei Ye, Poorvi Hebbbar, Abhinav Gupta, and Shubham Tulsiani. Diffusion-guided reconstruction of everyday hand-object interaction clips. In *Proceedings of the IEEE/CVF International Conference on Computer Vision*, pages 19717–19728, 2023. 2
- [36] Zhao-Heng Yin, Binghao Huang, Yuzhe Qin, Qifeng Chen, and Xiaolong Wang. Rotating without seeing: Towards in-hand dexterity through touch. *arXiv preprint arXiv:2303.10880*, 2023. 1, 2

- [37] Wenzhen Yuan, Siyuan Dong, and Edward H Adelson. Gelsight: High-resolution robot tactile sensors for estimating geometry and force. *Sensors*, 17(12):2762, 2017. 1
- [38] Qiang Zhang, Yunzhu Li, Yiyue Luo, Wan Shou, Michael Foshey, Junchi Yan, Joshua B Tenenbaum, Wojciech Matusik, and Antonio Torralba. Dynamic modeling of hand-object interactions via tactile sensing. In *2021 IEEE/RSJ International Conference on Intelligent Robots and Systems (IROS)*, pages 2874–2881. IEEE, 2021. 3
- [39] Yuxiao Zhou, Marc Habermann, Weipeng Xu, Ikhsanul Habibie, Christian Theobalt, and Feng Xu. Monocular real-time hand shape and motion capture using multi-modal data. In *Proceedings of the IEEE/CVF Conference on Computer Vision and Pattern Recognition*, pages 5346–5355, 2020. 4

## A. Flow Prediction Result

To validate the accuracy of our proposed flow prediction module (FPM), we report the Chamfer distance error on the DexYCB and HOT datasets in Tab. 4. The relatively low Chamfer distance demonstrates the efficacy of our network. The slightly better results on the DexYCB dataset are likely due to the larger hand-object movements and more challenging object deformations in the HOT dataset.

We also present some qualitative results in Fig. 6. The top section compares our predicted flow added to the last frame’s point cloud with the ground truth of the current frame’s point cloud. The near overlap of the two point clouds indicates high prediction accuracy. The bottom section shows a sequence of our estimation results, illustrating our method’s ability to track hand movements and object deformations in whole sequences.

Dataset	DexYCB		HOT	
Category	Box	Bottle	Sponge	Plasticine
CD(mm)↓	8.7	9.1	10.3	12.2

Table 4. Quantitative results for flow predictions in VDT-Net.

## B. Ablation Study, Extended

### B.1. Importance of flow prediction module

To demonstrate the importance of our flow prediction module (FPM), we conducted an experiment by directly fusing the visual features extracted from the input point clouds using the transformer fusion layer. The quantitative results are shown in Tab. 5. Introducing FPM significantly improves all scores, validating our feature fusion approach that incorporates the 3D static information of the current frame and the correspondence feature from the flow.

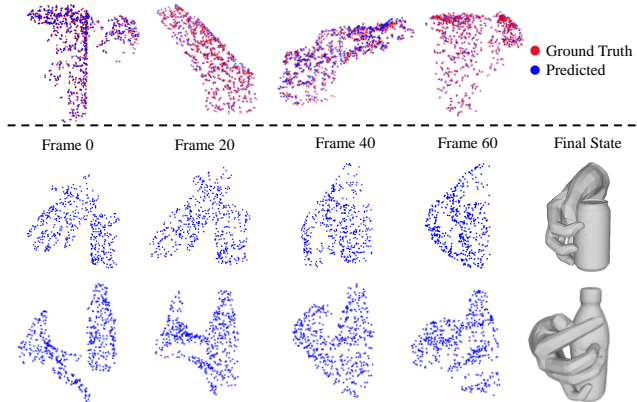


Figure 6. Qualitative results on flow prediction using FPM.

Metrics	IoU↑	CD↓	MPJPE↓
Dataset	DexYCB		
VDT(w/o FPM)	84.3	15.7	17.1
VDT	<b>90.1</b>	<b>9.6</b>	<b>13.2</b>
Dataset	HOT		
VDT(w/o FPM)	64.7	20.2	16.3
VDT	<b>80.5</b>	<b>10.9</b>	<b>13.6</b>

Table 5. Quantitative results on DexYCB and HOT Dataset for whether using the flow prediction module (denoted "FPM" in the table). "w/o" indicates without.

Metrics	MPJPE↓	PD↓	CloU↑	Iter. Time(s)↓
Keypoint	<b>11.3</b>	7.3	<b>40.3</b>	<b>3.5 ± 0.5</b>
All Verts	14.5	<b>6.9</b>	25.6	37 ± 3

Table 6. Quantitative results on evaluating point pair establishment on key points and on all-hand vertices.

### B.2. Different point pair establishment strategies

This section discusses the influence of two point pair establishment strategies: using **keypoints** or **all-hand vertices**. When considering all hand vertices, we establish point pairs between them and nearby object vertices, treating the force exerted by the hand as the reading from the nearest sensor. The quantitative results of these two methods are shown in Tab. 6. While penetration depth improves slightly, both contact IoU and MPJPE decrease. This is likely because considering all sensors leads to conflicting optimization directions for the same joint, as sensors within the same regions may experience different contact situations. Additionally, the iteration time increases about tenfold compared to our setting.